Photoexcited carrier dynamics and impact-excitation cascade in graphene

Photoexcited carrier dynamics and impact-excitation cascade in graphene

Justin C. W. Song,[1,2] Klaas J. Tielrooij,[3] Frank H. L. Koppens,[3] and Leonid S. Levitov[1]
[1]*Department of Physics, Massachusetts Institute of Technology, Cambridge, Massachusetts 02139, USA*
[2]*School of Engineering and Applied Sciences, Harvard University, Cambridge, Massachusetts 02138, USA*
[3]*ICFO-Institut de Ciéncies Fotóniques, Mediterranean Technology Park, Castelldefels (Barcelona) 08860, Spain*
(Received 21 September 2012; published 23 April 2013)

In materials with strong electron-electron interactions, photoexcitation can trigger a cascade in which multiple particle-hole excitations are generated. Here we analyze the cascade of impact-excitation processes in graphene in which many hot carriers are generated by a single absorbed photon. We show that the number of generated carriers has a strong dependence on doping (gate tunability). Linear scaling with photon energy is predicted for the number of pairs and for the duration of the cascade. These dependencies, along with a sharply peaked angular distribution of excited carriers, provide clear experimental signatures of hot carrier multiplication.

DOI: 10.1103/PhysRevB.87.155429 PACS number(s): 78.67.Wj, 78.20.Bh

I. INTRODUCTION

Converting light to electrical currents or voltages is a complex, multistep process which involves photoexcited particles and holes undergoing scattering by other charge carriers and by lattice vibrations. One of the key questions in the field of optoelectronics is identifying materials in which *carrier multiplication* can occur, i.e., a single absorbed photon yielding a large number of particle-hole pairs as a result of the primary photoexcited pair producing secondary pairs. Efficient carrier multiplication relies on a combination of characteristics such as a wide band of states with a large phase space density for pair excitations, strong electron-electron scattering, and not too strong electron-phonon interaction. While graphene is by no means a unique example of a system with these properties, it is believed to fit the bill better than other materials. This has motivated an intense investigation of photoexcitation processes in graphene-based systems.[1–12]

Graphene possesses a number of characteristics that distinguish it from other optoelectronic materials. One unique aspect of graphene is its truly two-dimensional structure which renders its electronic states fully exposed. Photogenerated carriers in such a system can in principle be extracted by a vertical transfer process, e.g., in a sandwich-type tunneling structure. Vertical carrier extraction eliminates carrier loss in lateral transport between the photoexcitation region and contacts, often a limiting factor for optoelectronic response in semiconductor systems.[13] Another distinguishing trait of graphene is slow electron-lattice cooling,[14–16] which leads to hot carrier cooling lengths reaching a few microns even at room temperature.[17,18] Slow cooling enhances hot-carrier effects, leading to a unique photocurrent generation mechanism.[17,19]

A number of experimental techniques have been employed to track the decay dynamics of photoexcited carriers in graphene, unraveling a complex picture of competing relaxation pathways.[1,3,5,6,9,20] In particular, a recent ultrafast optical pump-terahertz probe study[20] of doped graphene obtained detailed information on the number of hot carriers generated in the cascade following a short photoexcitation pulse. It was found that this number scales linearly with (i) the number of absorbed photons and (ii) the energy of individual photons. These dependencies indicate that the decay of photoexcited carriers is dominated by electron-electron scattering events rather than the emission of phonons (photoexcitation cascade dominated by phonon emission is not expected to show scaling with photon energy). These results, reproduced in Fig. 1(b), highlight the crucial role that interactions play in the photoexcitation cascade (and optical response) of graphene.

However, studies of interaction effects have mostly concentrated on undoped graphene. Theory predicts that the linear dispersion of charge carriers acquires a negative curvature due to electron-electron interactions, $d^2\epsilon(k)/dk^2 < 0$, which inhibits decay via electron-electron scattering in undoped graphene.[11,21] However, while the prediction of negative curvature appears to be in agreement with transport measurements,[22] ARPES experiments support the scenario of interaction-mediated decay[23,24] and pump-probe experiments point to the crucial role interactions play in the photoexcitation cascade;[20] interaction-induced quasiparticle decay remains the subject of ongoing debate.[11,12,25,26]

Here we focus on the photoexcitation cascade in doped graphene. We identify *impact excitation* (IE) as the scattering process [see intraband carrier-carrier scattering process in Fig. 1(a)] that dominates carrier relaxation dynamics in this system. Multiple secondary electron-hole (e-h) pairs produced by IE scattering involving a photoexcited carrier and ambient carriers in the Fermi sea can lead to efficient hot carrier multiplication. Our analysis predicts that IE processes result in a chainlike cascade consisting of sequential steps with relatively *small energy loss* per step $\Delta\epsilon \sim E_F$, where E_F is the Fermi energy in graphene doped away from neutrality [see Figs. 1(a) and 1(c)]. As we shall see, both the number of pairs produced in the cascade (hot carrier multiplication factor) and the characteristic energy for the pairs are highly sensitive to doping. As a result, the key parameters of photoexcitation cascade in graphene are expected to be gate tunable in a wide range.

As we argue below, the IE rate takes the highest values allowed by unitarity, $\Gamma \sim E_F/(2\pi\hbar)$ (these values are consistent with the inelastic lifetimes estimated in Refs. 26–28).

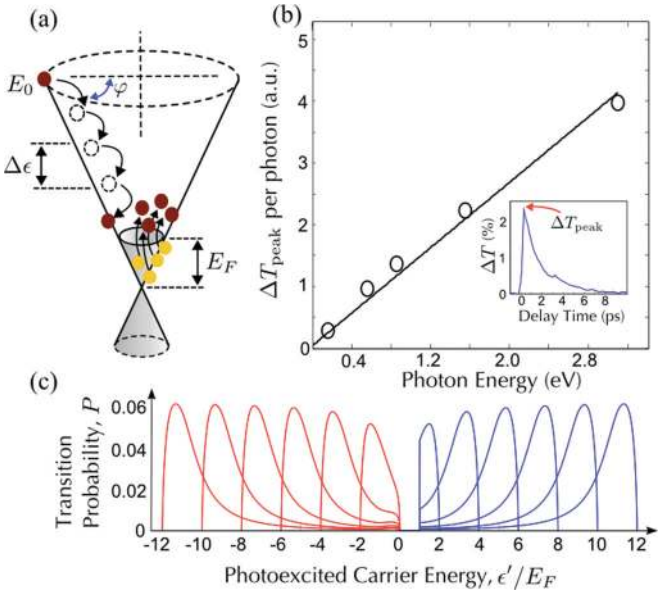

FIG. 1. (Color online) (a) Impact excitation (IE) cascade of a photoexcited carrier with initial energy E_0. Each cascade step involves electron-hole pair excitations with energy $\Delta\epsilon \sim E_F$, where E_F is Fermi energy. The net number of generated pairs and the relaxation rate depend strongly on E_F [see Eqs. (1) and (14)], and thus can be tuned by gate voltage. (b) Measured response in optical pump-terahertz probe of CVD graphene interpreted through the number of photogenerated hot carriers per photon. Typical experimental trace for differential transmission ΔT as a function of pump-probe delay time, shown in the inset, features a pronounced peak. The peak height is proportional to the number of generated hot carriers. Peak value $\Delta T_{\rm peak}$, normalized by absorbed photon density, is shown as a function of photon energy (adapted from Ref. 20). Note linear scaling of $\Delta T_{\rm peak}$ vs pump photon energy. (c) Transition probability (in units of $\hbar^{-1}$) obtained from Eq. (13). IE processes with different initial energies, $\epsilon_i/E_F = -12, -10, \ldots, 10, 12$ (here $\Delta\epsilon = \epsilon_i - \epsilon'$). Electron (hole) contributions shown by blue (red) curves.

This fast characteristic rate makes this scattering process a highly efficient relaxation pathway which dominates over phonon-mediated pathways in a wide range of energies. As a result, the photoexcitation cascade proceeds in a step-like fashion depicted in Figs. 1(a) and 1(c) producing multiple e-h pairs.

The dependence on excitation energy E_0 and Fermi energy E_F provides clear experimental signatures of this relaxation mechanism. In particular, the average number of e-h pairs produced in the cascade triggered by a *single photoexcited electron* is

$$\langle N\rangle = \int_{E_L}^{E_0} \frac{d\epsilon}{\langle\Delta\epsilon\rangle}, \quad \langle\Delta\epsilon\rangle = \frac{\mathcal{J}_{\rm el}(\epsilon)}{\Gamma(\epsilon)}, \tag{1}$$

where $\langle\Delta\epsilon\rangle$ is the average energy loss per step, and $\mathcal{J}_{\rm el}(\epsilon)$ and $\Gamma(\epsilon)$ are the IE energy-relaxation and scattering rates, respectively [see Eq. (14)]. Here $E_L \approx E_F$ is a low-energy cutoff corresponding to the energy below which IE processes are quenched; we used $E_L = 2E_F$ (see discussion below). Figure 2(a) indicates that $\langle N\rangle$ exceeds unity and grows quickly for E_0 above a few E_F (red curve). Since $\langle\Delta\epsilon\rangle \sim E_F$, we find that $\langle N\rangle$ scales as E_0/E_F. In particular, an

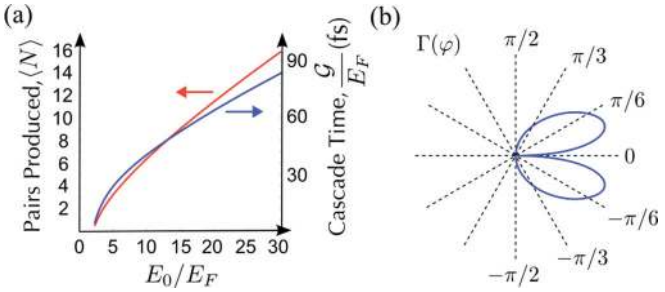

FIG. 2. (Color online) (a) Average net number of e-h pairs produced in the cascade triggered by a photoexcited electron with energy E_0 (red curve). Cascade duration, $\Delta t = \mathcal{G}/(E_F\,[\text{eV}])$ fs, see Eq. (2) (blue curve). (b) Angular dependence for the e-h excitation rate $\Gamma(\varphi)$, where φ is the angle between $\mathbf{k_1}$ and $\mathbf{q}$, see Fig. 3(a).

approximately linear dependence $\langle N\rangle \approx 0.55E_0/E_F$ is found for $E_0/E_F \gg 1$.

Similarly, the time it takes for the photoexcited electron to completely decay, Δt, also exhibits strong E_0 and E_F dependence. This fairly short time, on the order of hundreds of femtoseconds, is

$$\Delta t = \int_{E_L}^{E_0} \frac{d\epsilon}{\mathcal{J}_{\rm el}(\epsilon)} = \frac{\mathcal{G}(E_0/E_F)}{E_F[\text{eV}]}\ \text{fs}, \tag{2}$$

where $\mathcal{G}$ is a dimensionless scaling function [blue curve in Fig. 2(a)]. As shown in Fig. 2(a), $\mathcal{G}$ scales approximately linearly with E_0/E_F, yielding a Δt that scales linearly with the excitation energy. For a typical doping value of $E_F = 0.2$ eV and initial photoexcited carrier energy $E_0 = 1$ eV we find $\Delta t \approx 0.12$ ps, far faster than typical electron-lattice cooling time scales found in graphene.[14–16] This separation of time scales means that the energy relaxation cascade occurs independently of electron-lattice cooling.

Lastly, the angular distribution for impact-excitation transitions is highly anisotropic. This produces a strong search-light-type structure peaked along the preferred direction of momentum transfer shown in Fig. 2(b).

II. IMPACT EXCITATION SCATTERING

Our system is described by the Hamiltonian for $N = 4$ species of massless Dirac particles,

$$\mathcal{H} = \sum_{\mathbf{k},i} \psi^\dagger_{\mathbf{k},i}(v\sigma\cdot\mathbf{k})\psi_{\mathbf{k},i} + \mathcal{H}_{\text{el-el}}, \tag{3}$$

$$\mathcal{H}_{\text{el-el}} = \frac{1}{2}\sum_{\mathbf{q},\mathbf{k},\mathbf{k}',i,j} V(\mathbf{q})\psi^\dagger_{\mathbf{k}+\mathbf{q},i}\psi^\dagger_{\mathbf{k}'-\mathbf{q},j}\psi_{\mathbf{k}',j}\psi_{\mathbf{k},i}. \tag{4}$$

Here $i,j = 1\ldots N$ and $V(\mathbf{q}) = 2\pi e^2/|\mathbf{q}|\kappa$ is the Coulomb interaction. Importantly, transitions in a massless Dirac band governed by the Hamiltonian (3) are subject to certain kinematical constraints.[11,12] These constraints arise due to the combined effect of linear dispersion in two Dirac cones, $E_\pm(\mathbf{p}) = \pm v|\mathbf{p}|$, and the momentum conserving character of carrier scattering. Here we analyze the simplest case of a two-body collision. Each of the two particles participating in a collision can make transitions between states in the upper and lower Dirac cones which we denote by $+$ and $-$ respectively. Two kinds of transitions can be distinguished:

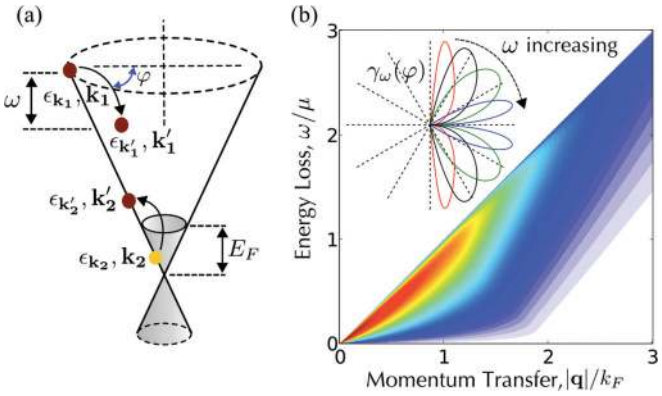

FIG. 3. (Color online) (a) Kinematics of intraband carrier-carrier scattering in doped graphene. A photoexcited electron makes the transition from $\mathbf{k_1}$ to $\mathbf{k}'_\mathbf{1}$ by exciting an electron-hole pair from the Fermi sea from $\mathbf{k_2}$ to $\mathbf{k}'_\mathbf{2}$. (b) Spectral function $R(\mathbf{q},\omega)$ of particle-hole excitation as a function of momentum transfer and energy transfer per scattering event. (inset) Angular distribution of normalized energy resolved transition rate [see Eq. (12) for fixed values of $\omega/E_F = 0.2,0.5,1,10$ (red, black, green, and blue curves, respectively)]. The near-collinear character of scattering at high ω is manifested in narrowing of the angular distribution.

intraband transitions ($+\to+$ or $-\to-$) and interband transitions ($+\to-$ or $-\to+$). Since momentum change in any transition satisfies $||\mathbf{p}_1|-|\mathbf{p}_2|| < |\mathbf{p}_1-\mathbf{p}_2| < |\mathbf{p}_1|+|\mathbf{p}_2|$, the intraband transitions can only occur when the energy and momentum change are related by $|\Delta\epsilon| \leqslant v|\Delta p|$, whereas the interband transitions are possible only when $|\Delta\epsilon| \geqslant v|\Delta p|$.

The scattering process of interest, pictured in Fig. 3(a), involves a photoexcited carrier with high energy and momentum $\epsilon_{\mathbf{k}_1} \gg E_F$, $|\mathbf{k}_1| \gg k_F$, which is scattered to a lower energy state having momentum $\mathbf{k}'_1$ with recoil momentum $\mathbf{q} = \mathbf{k_1} - \mathbf{k}'_1$ given to an electron in the Fermi sea. The latter process results in a particle-hole pair excitation, as depicted by a transition from $\mathbf{k_2}$ to $\mathbf{k}'_2$ in Fig. 3(a). The transition rate for this process, evaluated by the standard golden rule approach, takes the form

$$W_{\mathbf{k}'_1,\mathbf{k}_1} = \frac{2\pi N}{\hbar}\sum_{\mathbf{q},\mathbf{k}_2,\mathbf{k}'_2} f_{\mathbf{k}_2}\left(1-f_{\mathbf{k}'_2}\right)F_{\mathbf{k}_2,\mathbf{k}'_2}|\tilde{V}_\mathbf{q}|^2 \times \delta_{\mathbf{k}'_1,\mathbf{k}_1+\mathbf{q}}\delta_{\mathbf{k}'_2,\mathbf{k}_2-\mathbf{q}}\delta\left(\epsilon_{\mathbf{k}'_1}-\epsilon_{\mathbf{k}_1}+\epsilon_{\mathbf{k}'_2}-\epsilon_{\mathbf{k}_2}\right). \quad (5)$$

Here $f_\mathbf{k}$ is a Fermi function, and $F_{\mathbf{k},\mathbf{k}'} = |\langle \mathbf{k}'s'|\mathbf{k}s\rangle|^2$ is the coherence factor ($s,s' = \pm$ label states in the electron and hole Dirac cones). We treat the Coulomb interaction which mediates scattering between the photoexcited carrier and the carriers in the Fermi sea by accounting for dynamical screening in the RPA approximation:

$$\tilde{V}_\mathbf{q} = \frac{V^0_\mathbf{q}}{\varepsilon(\omega,\mathbf{q})}, \quad \varepsilon(\omega,\mathbf{q}) = 1 - V^0_\mathbf{q}\Pi(\mathbf{q},\omega), \quad (6)$$

where $V^0_\mathbf{q} = 2\pi e^2/|\mathbf{q}|\kappa$ and $\varepsilon(\omega,\mathbf{q})$ describes dynamical screening. Here Π is the polarization operator

$$\Pi(\mathbf{q},\omega) = N\sum_{\mathbf{k},s,s'} F_{\mathbf{k},\mathbf{k}+\mathbf{q};ss'}\frac{f(\epsilon_{\mathbf{k},s})-f(\epsilon_{\mathbf{k}+\mathbf{q},s'})}{\omega+\epsilon_{\mathbf{k},s}-\epsilon_{\mathbf{k}+\mathbf{q},s'}+i0}, \quad (7)$$

with band indices $s,s' = \pm$. This includes both intra- ($s = s'$) and inter- ($s \neq s'$) band contributions.[29]

For Eq. (5) to give a nonvanishing result, the transitions $\mathbf{k}_1 \to \mathbf{k}'_1$, $\mathbf{k}_2 \to \mathbf{k}'_2$ must occur in like pairs, both intraband or both interband. Since $\mathbf{k}_1 \to \mathbf{k}'_1$ is restricted to be within a single band, $\mathbf{k}_2 \to \mathbf{k}'_2$ must also be intraband. As a result, relaxation via interband scattering is blocked, whereas intraband scattering is allowed. Kinematical blocking of interband processes can in principle be relieved by three-body (or higher-order) collisions (not discussed here). Such processes may become important at strong excitation, however they are expected to be weak in the low excitation power regime.

As shown below, the typical energy of an excited pair is much smaller than the photoexcitation energy $\epsilon_{\mathbf{k}_1}$. Anticipating this result, it is convenient to factorize the transition rate by expressing it through the spectrum of secondary pair excitations. This can be accomplished by writing $\delta(\epsilon_{\mathbf{k}'_1}-\epsilon_{\mathbf{k}_1}+\epsilon_{\mathbf{k}'_2}-\epsilon_{\mathbf{k}_2}) = \int_{-\infty}^{\infty} d\omega\delta(\epsilon_{\mathbf{k}'_1}-\epsilon_{\mathbf{k}_1}+\omega)\delta(\epsilon_{\mathbf{k}'_2}-\epsilon_{\mathbf{k}_2}-\omega)$.[30] Next, we use the identity $f_{\mathbf{k}_2}(1-f_{\mathbf{k}'_2}) = (f_{\mathbf{k}_2}-f_{\mathbf{k}'_2})\times(N(\epsilon_{\mathbf{k}'_2}-\epsilon_{\mathbf{k}_2})+1)$, where $N(\omega) = 1/(e^{\omega/k_BT}-1)$ is the Bose function taken at the electron temperature. Lastly, we express the sum of $(f_{\mathbf{k}_2}-f_{\mathbf{k}'_2})\delta(\epsilon_{\mathbf{k}'_2}-\epsilon_{\mathbf{k}_2}-\omega)$ through a suitably defined susceptibility

$$\chi''(\mathbf{q},\omega) = N\sum_\mathbf{k} F_{\mathbf{k},\mathbf{k}+\mathbf{q}}(f_\mathbf{k}-f_{\mathbf{k}+\mathbf{q}})\delta(\epsilon_{\mathbf{k}+\mathbf{q}}-\epsilon_\mathbf{k}-\omega), \quad (8)$$

which can also be written as $\chi''(\mathbf{q},\omega) = -\frac{1}{\pi}\,\mathrm{Im}\,\Pi(\mathbf{q},\omega)$. This yields a compact and intuitive expression for the total scattering rate:

$$\Gamma = \sum_{\mathbf{k}'_1} W_{\mathbf{k}'_1,\mathbf{k}_1}\left(1-f_{\mathbf{k}'_1}\right)F_{\mathbf{k}_1,\mathbf{k}'_1} = \int_{-\infty}^{\infty} d\omega P(\omega), \quad (9)$$

$$P(\omega) = A\sum_\mathbf{q}|\tilde{V}_\mathbf{q}|^2 F_{\mathbf{k}_1,\mathbf{k}'_1}\chi''(\mathbf{q},\omega)\delta\left(\epsilon_{\mathbf{k}'_1}-\epsilon_{\mathbf{k}_1}+\omega\right), \quad (10)$$

where $A = \frac{2\pi}{\hbar}[N(\omega)+1)][1-f(\epsilon_{\mathbf{k}_1}-\omega)]$ and $\mathbf{k}'_1 = \mathbf{k}_1 - \mathbf{q}$.

As we show below, the typical energy and momentum transferred per scattering is of the order of E_F and E_F/v, respectively. These values are much smaller than those of the photoexcited electron. We can therefore approximate $F_{\mathbf{k}_1,\mathbf{k}'_1} \approx 1$, $f(\epsilon_{\mathbf{k}_1}-\omega) \approx 0$ and write the delta function as $\delta(\epsilon_{\mathbf{k}'_1}-\epsilon_{\mathbf{k}_1}+\omega) \approx \delta(v|\mathbf{q}|\cos\varphi-\omega)$, where φ is the angle between $\mathbf{k}_1$ and $\mathbf{q}$. The approximation $|\mathbf{q}| \ll |\mathbf{k}_1|, |\omega| \ll v|\mathbf{k}_1|$ is appropriate under realistic conditions: for example, visible light frequencies translate to $\epsilon_\mathbf{k} = hf/2 = 750$ meV, which is considerably larger than E_F for typical doping values. Equation (9) then yields the angle dependent transition rate

$$\Gamma(\varphi) = \int_{-\infty}^{\infty} d\omega\gamma_\omega(\varphi), \quad (11)$$

$$\gamma_\omega(\varphi) = \int\frac{d^2q}{(2\pi)^2}R(\mathbf{q},\omega)\delta(v|\mathbf{q}|\cos\varphi-\omega), \quad (12)$$

where $R(\mathbf{q},\omega) = A|\tilde{V}_\mathbf{q}|^2\chi''(\mathbf{q},\omega)$. We evaluate the spectral function $R(\mathbf{q},\omega)$ using the RPA-screened interaction, Eq. (6), and susceptibility expressed through the polarization function from Ref. 29 and the interaction parameter $\alpha = e^2/(\kappa\hbar v) = 0.73$. The angular distribution $\Gamma(\varphi)$, as well as the energy resolved distribution $\gamma_\omega(\varphi)$, feature interesting angular patterns [see Figs. 2(b) and 3 (inset)]. Note in particular a sharp search-light-type structure corresponding to the preferred direction

of momentum transfer $\mathbf{q}$ in the IE process. The peaks move closer to $\varphi = 0$ as ω increases, indicating that carrier-carrier scattering with high energy transfer is nearly collinear. This is analogous to the radiation pattern for an ultrarelativistic particle becoming focused along particle velocity.[31]

The same approach can be used to obtain the energy spectrum of pair excitations. In the following, however, we study the *full energy dependence* of $P(\Delta\epsilon)$ not limiting ourselves to the asymptotic behavior at high photoexcited energies. Using a Jacobian to convert the delta function in energy to a delta function in angles in Eq. (10), we perform the angular integral in Eq. (10) to obtain

$$P(\Delta\epsilon) = \int_0^\infty \frac{2|\mathbf{k_1}| - (\Delta\epsilon/v\hbar) - |\mathbf{q}|\cos\varphi}{(2\pi)^2|\mathbf{k_1}||\mathbf{q}|\hbar v \sin\varphi} R(\mathbf{q},\Delta\epsilon) q dq, \tag{13}$$

where φ is the angle between $\mathbf{k_1}$ and $\mathbf{q}$ and satisfies $(|\mathbf{k_1}|^2 - 2|\mathbf{k_1}||\mathbf{q}|\cos\varphi + |\mathbf{q}|^2)^{1/2} - |\mathbf{k_1}| = \Delta\epsilon/(v\hbar)$. Numerically integrating Eq. (13) and taking $\epsilon \gg k_B T$ yields transition probabilities $P(\Delta\epsilon)$ shown in Fig. 1(c) for different initial photoexcited energies $\epsilon_i = \epsilon_{\mathbf{k}_1}$. We find that $P(\Delta\epsilon)$ peaks close to $\Delta\epsilon \approx E_F$ and decay rapidly for $\Delta\epsilon \gg E_F$. This nonmonotonic dependence arises from the competition between the available phase space, which grows with $\Delta\epsilon$, and the Coulomb interaction form factor, which decreases with $|\mathbf{q}|$.

The efficiency of IE scattering can be linked to the large values of E_F in graphene. The relation between efficiency and E_F can be clarified by simple dimensional analysis. We note that $P(\Delta\epsilon)$ depends on $\Delta\epsilon$ essentially via the dimensionless parameter $x = \Delta\epsilon/E_F$. This is clearly seen, e.g., from pair excitation spectrum shown for different values of initial energy $\epsilon_i = \epsilon_{\mathbf{k}_1}$ in Fig. 1(c): The width and profile of $P(\Delta\epsilon)$ has a very weak dependence on ϵ_i. This can be captured by writing the scattering rate Γ [Eq. (9)] as well as the energy relaxation rate $\mathcal{J}_{\rm el} = \int_{-\infty}^{\infty} \Delta\epsilon P(\Delta\epsilon) d\Delta\epsilon$ in the form

$$\Gamma(\epsilon) = \frac{E_F}{\hbar}\int_0^{\epsilon/E_F} \tilde{P}(x)dx, \quad \mathcal{J}_{\rm el}(\epsilon) = \frac{E_F^2}{\hbar}\int_0^{\epsilon/E_F} x\tilde{P}(x)dx, \tag{14}$$

where we introduced dimensionless $\tilde{P}(x) = \hbar P(\Delta\epsilon)$.

The E_F dependencies in Eq. (14) manifest in observables such as the average number of secondary e-h pairs produced in a single photoexcitation cascade, $\langle N\rangle$, and its total cascade time, Δt. These quantities are related via $\langle N\rangle = \int_0^{\Delta t}\Gamma dt$. Using $d\epsilon/dt = -\mathcal{J}_{\rm el}(\epsilon)$ combined with Eq. (14), we obtain Eq. (1) for $\langle N\rangle$ and Eq. (2) for Δt. In both cases, we used a low energy cutoff for the energy below which IE processes are quenched, $E_L \approx E_F$. Below the energy E_L, the relaxation and scattering of the carrier from impact excitation slows dramatically and other relaxation processes dominate, for example energy relaxation via the emission of acoustic phonons. In evaluating Eqs. (1) and (2), we used the value $E_L = 2E_F$ below which the predicted value Δt rapidly increases. The scaling of Δt and $\langle N\rangle$ with both excitation energy E_0 and doping in Fig. 2(a) are clear experimental signatures of IE. Currently, particle-hole pair production and cascade times are the subject of intense experimental interest.[20,32,33]

III. COMPARISON WITH PHONON EMISSION

Here we compare energy relaxation from IE processes with the contribution of other potentially significant channels. In particular, electron-phonon scattering leads to a direct transfer of energy to the lattice degrees of freedom without creation of secondary electron-hole excitations. We focus on the contribution of optical phonons, which under normal circumstances is more important than that of acoustic phonons. Our estimate shows that under realistic conditions the contribution of optical phonons to the energy relaxation rate is weaker than that due to carrier-carrier scattering, $\mathcal{J}_{\rm ph} \lesssim \mathcal{J}_{\rm el}$. This energy relaxation channel was discussed in Ref. 20. We reproduce these results for the reader's convenience. The transition rate due to electron-phonon scattering can be described by Fermi's golden rule

$$W^{\text{el-ph}}_{\mathbf{k}',\mathbf{k}} = \frac{2\pi N}{\hbar}\sum_{\mathbf{q}} |M(\mathbf{k}',\mathbf{k})|^2 \delta(\Delta\epsilon_{\mathbf{k}',\mathbf{k}} + \omega_{\mathbf{q}}) \times \delta_{\mathbf{k}',\mathbf{k}+\mathbf{q}}(N(\omega_{\mathbf{q}})+1),$$
$$\Delta\epsilon_{\mathbf{k}',\mathbf{k}} = \epsilon_{\mathbf{k}'} - \epsilon_{\mathbf{k}}, \tag{15}$$

where $\omega_{\mathbf{q}} = \omega_0 = 200$ meV is the optical phonon dispersion relation, and $N(\omega_{\mathbf{q}})$ is a Bose function. Here $\mathbf{k}$ is the initial momentum of the photoexcited electron, $\mathbf{k}'$ is the momentum it gets scattered into, and $\mathbf{q}$ is the momentum of the optical phonon. The electron-phonon matrix element $M(\mathbf{k}',\mathbf{k})$ is

$$|M(\mathbf{k}',\mathbf{k})|^2 = g_0^2 F_{\mathbf{k},\mathbf{k}'}, \quad g_0 = \frac{2\hbar^2 v}{\sqrt{2\rho\omega_0 a^4}}, \tag{16}$$

where $F_{\mathbf{k},\mathbf{k}'}$ is the coherence factor for graphene, g_0 is the electron-optical phonon coupling constant,[14] ρ is graphene's mass density, and $a = 1.42$ Å is the distance between nearest neighbor carbon atoms. The energy-loss rate of the photoexcited carrier at energy ϵ due to the emission of an optical phonon is

$$\mathcal{J}_{\rm ph}(\epsilon) = \sum_{\mathbf{k}'} W^{\text{el-ph}}_{\mathbf{k}',\mathbf{k}}(\epsilon'_k - \epsilon)[1 - f(\epsilon_{\mathbf{k}'})]. \tag{17}$$

Integrating over $\mathbf{q}$ and $\mathbf{k}'$ we obtain

$$\mathcal{J}_{\rm ph}(\epsilon) = \frac{\pi N}{\hbar}\omega_0 g_0^2 [1 - f(\epsilon - \omega_0)](N(\omega_0)+1)\nu(\epsilon - \omega_0), \tag{18}$$

where $\nu(\epsilon) = \epsilon/(2\pi v^2\hbar^2)$ is the electron density of states in graphene. Hence, $\mathcal{J}_{\rm ph}(\epsilon)$ varies linearly with the photoexcited carrier energy $\epsilon > \omega_0$ and vanishes for $\epsilon < \omega_0$. Because the electron-phonon coupling with optical phonon is a constant, this result is to be expected from the increased phase space to scatter into at higher photoexcited carrier energy.

To get an estimate of the energy relaxation rate, we estimate $[N(\omega_0)+1] \approx 1$ and $1 - f(\epsilon - \omega_0) \approx \Theta(\epsilon - \omega_0 - E_F)$ to obtain

$$\mathcal{J}_{\rm ph}(\epsilon) \approx \frac{\epsilon - \omega_0}{\tau_0}\Theta(\epsilon - \omega_0 - E_F), \quad \tau_0 = \frac{2v^2\hbar^3}{N\omega_0 g_0^2}. \tag{19}$$

Using $\rho = 7.6\times 10^{-11}$ kg cm^{-2}, we find $\tau_0 \approx 734$ fs.

Using $P(\Delta\epsilon)$ evaluated from Eq. (13), we can compare the IE energy relaxation rate $\mathcal{J}_{\rm el}$ with the energy-loss rate due to optical phonons $\mathcal{J}_{\rm ph}$. As illustrated in Fig. 4, for a typical

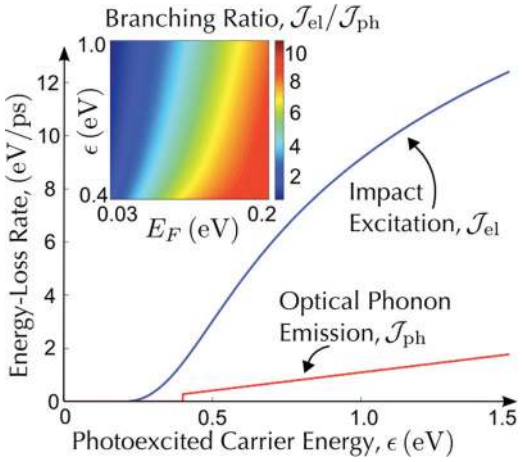

FIG. 4. (Color online) Energy-loss rate via impact excitation, $\mathcal{J}_{el}$ [blue curve, see Eq. (14)], and optical phonon emission, $\mathcal{J}_{ph}$ [red curve, see Eq. (19)] for a typical doping of $E_F = 0.2$ eV. (Inset) Branching ratio, $\mathcal{J}_{el}/\mathcal{J}_{ph}$ vs. ϵ and E_F. Note that the branching ratio can be tuned over an order of magnitude by density dependence.

doping of $E_F = 0.2$ eV, the rate $\mathcal{J}_{el}$ overwhelms the rate $\mathcal{J}_{ph}$ over the entire spectrum of photoexcited carrier energies. We also analyzed the branching ratio $\mathcal{J}_{el}/\mathcal{J}_{ph}$ shown in the inset of Fig. 4 as a function of carrier density and photoexcited carrier energy. Interestingly, the density dependence of $\mathcal{J}_{el}$ translates into gate-tunable branching ratio $\mathcal{J}_{el}/\mathcal{J}_{ph}$. For realistic gate voltage values, the branching ratio can vary by up to an order of magnitude.

IV. SUMMARY

As demonstrated above, the interaction mediated cascade of IE processes in doped graphene can lead to the generation of multiple electron-hole excitations by a single absorbed photon. We developed a detailed model to describe multiple pair generation in the IE cascade. Our analysis indicates that the number of pairs generated scales approximately linearly with photoexcitation energy. Similarly, the total cascade time also exhibits a linear scaling with photoexcitation energy. A comparison with electron-phonon scattering indicates that the IE scattering is very efficient and can dominate carrier relaxation for typical dopings. The predicted dependencies, as well as a sharply peaked angular distribution of e-h pairs, provide clear experimental signatures for IE-dominated cascade. Strong gate dependence of the cascade parameters affords a useful knob for the control of ultrafast scattering processes in graphene.

ACKNOWLEDGMENTS

We acknowledge financial support from the NSS program, Singapore (JS), the Office of Naval Research Grant No. N00014-09-1-0724 (LL), and Fundacio Cellex Barcelona (FK) and an NWO Rubicon Grant (KJT).

[1]T. Kampfrath, L. Perfetti, F. Schapper, C. Frischkorn, and M. Wolf, Phys. Rev. Lett. **95**, 187403 (2005).
[2]S. Butscher, F. Milde, M. Hirtschulz, E. Malić, and A. Knorr, Appl. Phys. Lett. **91**, 203103 (2007).
[3]P. A. George, J. Strait, J. Dawlaty, S. Shivaraman, M. Chandrashekhar, F. Rana, and M. G. Spencer, Nano Lett. **8**, 4248 (2008).
[4]F. T. Vasko and V. Ryzhii, Phys. Rev. B **77**, 195433 (2008).
[5]M. Breusing, C. Ropers, and T. Elsaesser, Phys. Rev. Lett. **102**, 086809 (2009).
[6]C. H. Lui, K. F. Mak, J. Shan, and T. F. Heinz, Phys. Rev. Lett. **105**, 127404 (2010).
[7]T. Winzer, A. Knorr, and E. Malić, Nano Lett. **10**, 4839 (2010).
[8]R. Kim, V. Perebeinos, and P. Avouris, Phys. Rev. B **84**, 075449 (2011).
[9]S. Winnerl, M. Orlita, P. Plochocka, P. Kossacki, M. Potemski, T. Winzer, E. Malic, A. Knorr, M. Sprinkle, C. Berger, W. A. de Heer, H. Schneider, and M. Helm, Phys. Rev. Lett. **107**, 237401 (2011).
[10]T. Winzer and E. Malić, Phys. Rev. B **85**, 241404 (2012).
[11]M. S. Foster and I. L. Aleiner, Phys. Rev. B **79**, 085415 (2009).
[12]F. Rana, Phys. Rev. B **76**, 155431 (2007).
[13]R. T. Ross and A. J. Nozik, J. Appl. Phys. **53**, 3813 (1982).
[14]R. Bistritzer and A. H. MacDonald, Phys. Rev. Lett. **102**, 206410 (2009).
[15]W.-K. Tse and S. Das Sarma, Phys. Rev. B **79**, 235406 (2009).
[16]J. C. W. Song, M. Y. Reizer, and L. S. Levitov, Phys. Rev. Lett. **109**, 106602 (2012).
[17]N. M. Gabor, J. C. W. Song, Q. Ma, N. L. Nair, T. Taychatanapat, K. Watanabe, T. Taniguchi, L. S. Levitov, and P. Jarillo-Herrero, Science **334**, 648 (2011).
[18]M. W. Graham, S.-F. Shi, D. C. Ralph, J. Park, and P. L. McEuen, Nat. Phys. **9**, 103 (2013).
[19]D. Sun, G. Aivazian, A. M. Jones, J. S. Ross, W. Yao, D. Cobden, and X. Xu, Nat. Nanotechnol. **7**, 114 (2012).
[20]K. J. Tielrooij, J. C. W. Song, S. A. Jensen, A. Centeno, A. Pesquera, A. Zurutuza Elorza, M. Bonn, L. S. Levitov, and F. H. L. Koppens, Nat. Phys. **9**, 248 (2013).
[21]J. Gonzalez, F. Guinea, and M. A. H. Vozmediano, Nucl. Phys. B **424**, 595 (1994).
[22]D. C. Elias, R. V. Gorbachev, A. S. Mayorov, S. V. Morozov, A. A. Zhukov, P. Blake, L. A. Ponomarenko, I. V. Grigorieva, K. S. Novoselov, F. Guinea, and A. K. Geim, Nat. Phys. **7**, 701 (2011).
[23]S. Y. Zhou, G.-H. Gweon, J. Graf, A. V. Fedorov, C. D. Spataru, R. D. Diehl, Y. Kopelevich, D.-H. Lee, Steven G. Louie, and A. Lanzara, Nat. Phys. **2**, 595 (2006).
[24]A. Bostwick, T. Ohta, T. Seyller, K. Horn, and E. Rotenberg, Nat. Phys. **3**, 36 (2007).
[25]M. Polini (private communication).

[26]D. M. Basko, S. Piscanec, and A. C. Ferrari, Phys. Rev. B **80**, 165413 (2009).
[27]E. H. Hwang, Ben Yu-Kuang Hu, and S. Das Sarma, Phys. Rev. B **76**, 115434 (2007).
[28]M. Polini, R. Asgari, G. Borghi, Y. Barlas, T. Pereg-Barnea, and A. H. MacDonald, Phys. Rev. B **77**, 081411 (2008).
[29]E. H. Hwang and S. Das Sarma, Phys. Rev. B **75**, 205418 (2007).
[30]G. F. Giuliani and J. J. Quinn, Phys. Rev. B **26**, 4421 (1982).
[31]J. D. Jackson, *Classical Electromagnetism*, 3rd ed. (Wiley, New York, 1999), pp. 668–669.
[32]R. D. Schaller and V. I. Klimov, Phys. Rev. Lett. **92**, 186601 (2004).
[33]M. C. Beard, G. M. Turner, and C. A. Schmuttenmaer, Phys. Rev. B **62**, 15764 (2000).